Acta Pharmaceutica Sinica B 2026;16(6):3892−3906

Chinese Pharmaceutical Association
Institute of Materia Medica, Chinese Academy of Medical Sciences

Acta Pharmaceutica Sinica B

www.elsevier.com/locate/apsb
www.sciencedirect.com

ORIGINAL ARTICLE

Interleukin 12-tethered nano-aluminum adjuvant orchestrates environmental immunomodulation to empower cytotoxic T cells against solid tumors

Aining Shen[a,b,†], Jing Zhao[a,b,†], Zhenwei Su[b], Ran Wang[b], Ying Li[b], Chaojie Zhu[c], Qingyuan Zhao[a], Pinwan Yu[a], Zhi Ping Xu[a,b,*], Lingxiao Zhang[a,b,d,*]

[a]*School of Medicine, Hangzhou City University, Hangzhou 310015, China*
[b]*Institute of Chemical Biology, Shenzhen Bay Laboratory, Shenzhen 518107, China*
[c]*Department of Hepatobiliary and Pancreatic Surgery the Second Affiliated Hospital, School of Medicine, Zhejiang University, Hangzhou 310009, China*
[d]*Interdisciplinary Nanoscience Center (INANO), Aarhus University, Aarhus C 8000, Denmark*

Received 6 August 2025; received in revised form 29 August 2025; accepted 7 September 2025

KEY WORDS

Nano-aluminum adjuvants;
Interleukin-12 tumor therapy;
Acidosis alleviation;
Mg^{2+} supplementation;
Cytotoxic T cell activation;
Cytotoxic T cell infiltration;
Cytotoxic T cell immune

Abstract The immunosuppressive tumor microenvironment (TME) profoundly limits the therapeutic efficacy of $CD8^+$ T cells in solid tumors. While cytokine therapies have shown promise in reactivating $CD8^+$ T cells, they fail to address the common suppressive environmental attributes (*e.g.*, acidosis and Mg^{2+} deficiency) of solid tumors. Here, we report an innovative $CD8^+$ T cell dual-functional modulator, interleukin-12-tethered nano-aluminum adjuvant (IL12@NAM), which counteracts the acidic TME to relieve acidosis and concurrently releases Mg^{2+} and IL12. Locally released Mg^{2+} and IL12 synergize in T cell infiltration and activation by promoting the phosphorylation of focal adhesion kinase and extracellular signal-regulated kinase 1/2, and enhance $CD8^+$ T cell activation and functions *via* the Ca^{2+}−nuclear factor of activated T cells 2 pathway. Furthermore, dual-functional IL12@NAM mitigates $CD8^+$ T cell exhaustion by reducing PD1 and LAG3 expression and effectively increases the differentiation towards T helper 1 cells while decreasing regulatory T cells, creating a more favorable immune network for enhanced $CD8^+$ T cell-mediated anti-tumor immunity. As a result, IL12@NAM has

*Corresponding authors.
E-mail addresses: zhanglx@inano.au.dk (Lingxiao Zhang); gordonxu@szbl.ac.cn (Zhi Ping Xu),
[†]These authors made equal contributions to this work.
Peer review under the responsibility of Chinese Pharmaceutical Association and Institute of Materia Medica, Chinese Academy of Medical Sciences.

https://doi.org/10.1016/j.apsb.2025.10.021

exhaustion;
Tumor microenvironment

demonstrated potent therapeutic efficacy against advanced melanoma and breast cancer, and remarkably empowered adoptive T therapy of solid tumors. This study provides a paradigm for empowering cytotoxic T cells by reactivating and creating a sustainable immunoresponsive environment, offering a potential adjuvant strategy to enhance solid tumor therapy.

1. Introduction

While immune checkpoint blockade and cytokine therapy effectively activate $CD8^+$ T cells[1,2], these therapeutics fail to preserve their effector functions in cases of tumor acidosis and metal ion dysregulation[3-5]. Tumor acidosis suppresses $CD8^+$ T cell infiltration and activity within the tumor microenvironment (TME). This acidic environment restricts nutrient uptake and promotes regulatory T cell (Treg) expansion, further driving $CD8^+$ T cell inactivation[6]. Acidosis also contributes to collagen accumulation around the tumors and further induces mechanical exhaustion of $CD8^+$ T cells[7,8]. Furthermore, deficiencies in essential metal ions (*e.g.*, Mg^{2+}, Li^+) not only impair the cytotoxicity of $CD8^+$ T cells and hinder lactate utilization as carbon source, but also promote tumor lactic acid production to exacerbate acidosis[9-11]. Consequently, tumor acidosis and metal ion imbalance have emerged as critical environmental factors that govern $CD8^+$ T cell recruitment, activation, persistence, and functions within the TME.

Magnesium-aluminum layered double hydroxide NanoAlum (NA), engineered from clinically used aluminum oxyhydroxide adjuvant and magnesium hydroxide antacid, has emerged as a novel immunomodulator for activating $CD8^+$ T cells within the TME[12]. With a chemical composition similar to the clinical antacid Talcid, NA effectively neutralizes excess lactic acid within the TME for up to two weeks following local injection[13]. During this process, pH is elevated and Mg^{2+} is continuously released from NA, transitioning the TME from an immunologically 'cold' state (where most $CD8^+$ T cells are inactive with limited infiltration into tumor tissues) to a 'cold-to-hot intermediate' state (where partially activated $CD8^+$ T cells infiltrate into tumor tissues)[14]. Although tumor acidosis alleviation and Mg^{2+} supplementation can facilitate $CD8^+$ T cell infiltration into tumors, the absence of T cell-specific immunological stimulation (*e.g.*, chemokines, cytokines) continues to hinder the restoration of their effector functions[14,15]. Furthermore, it remains unclear whether Mg^{2+}-mediated immune stimulation induces $CD8^+$ T cell exhaustion, similar to that observed with pro-inflammatory cytokines.

Interleukin 12 (IL12) is a promising pro-inflammatory cytokine that powerfully recruits and activates $CD8^+$ T cells[16-20]. IL12 also selectively recruits and expands adoptively transferred $CD8^+$ T cells within the TME[21]. Moreover, IL12 promotes the differentiation of $CD4^+$ T cells from T helper 2 (Th2) to Th1 effectors[15,16]. However, severe systemic side effects are also observed in clinical trials, which greatly hinder the direct application of IL12[22], underscoring the need for local and sustained administration. Recent strategies, such as IL12-tethered aluminum oxyhydroxide adjuvant[23], self-replicating IL12 RNA encapsulated oncolytic nanoparticles[24], and IL12 messenger RNA encapsulated extracellular vesicles[25], have successfully confined IL12 delivery around the TME. Despite these advances in delivery systems to address the cytokine delivery to immunologically activate T cells, $CD8^+$ T cells still face the hostile TME featured with tumor acidosis and metal ion dysregulation, which limits T cell infiltration, activation, persistence and functions[26].

Herein, we present an IL12-tethered NA (IL12@NAM) designed for simultaneous environmental and immunological activation of $CD8^+$ T cells within the immunosuppressive TME. As illustrated in Scheme 1, peritumorally injected IL12@NAM effectively elevates the pH and Mg^{2+} supplement in the TME (environmental) while releasing IL12 (immunological) to activate and preserve the effector functions of $CD8^+$ T cells. In terms of mechanism, NAM releases Mg^{2+} to activate the effector functions of $CD8^+$ T cells by enhancing lymphocyte function-associated antigen 1 (LFA1) mediated signaling, including proximal (focal adhesion kinase (FAK) phosphorylation) and distal (extracellular signal-regulated protein kinase 1/2 (ERK1/2) phosphorylation) activation. Simultaneously, the synergistic effect between Mg^{2+} and IL12 amplifies $CD8^+$ T cell activation and functions *via* the Ca^{2+}-nuclear factor of activated T cells 2 (NFAT2) pathway. Furthermore, IL12@NAM mitigates $CD8^+$ T cell exhaustion through reducing PD1 expression that was caused by the released IL12 and Mg^{2+}, promoting the differentiation of T helper towards Th1 phenotype, and reducing the Treg level. NA functions not only as a carrier for IL12 delivery but also as an amplifier that enhances IL12 functions. Our study introduces a new paradigm in tumor immunotherapy, showcasing the dual-functional IL12@NAM as an innovative approach to enviro-immunologically upregulate $CD8^+$ T cell infiltration and effector functions, not only activating and preserving their cytotoxicity but also preventing their inactivation and exhaustion.

2. Methods

2.1. Materials and reagents

Materials and reagents used in this study are listed in Supplementary Tables S1 and S2 with all corresponding details.

2.2. Cell lines

B16F10 melanoma cells and 4T1 triple negative breast cancer cells were obtained from American Type Culture Collection (ATCC) and cultured in RPMI 1640 containing with 10% (*v*/*v*) of fetal bovine serum (FBS) and 1% (*v*/*v*) of penicillin−streptomycin in an incubator at 37 °C with 5% (*v*/*v*) of carbon dioxide. $CD8^+$ T cells were obtained from spleens and lymph nodes of female C57BL/6 mice (6−8 weeks old) and isolated by EasySep Mouse $CD8^+$ T Cell Isolation Kit (#19853, Stem Cell, Canada). $CD8^+$ T cells were cultured and activated in RPMI 1640 containing 10% (*v*/*v*) of FBS, 1% (*v*/*v*) of penicillin−streptomycin, 50 μmol/L of

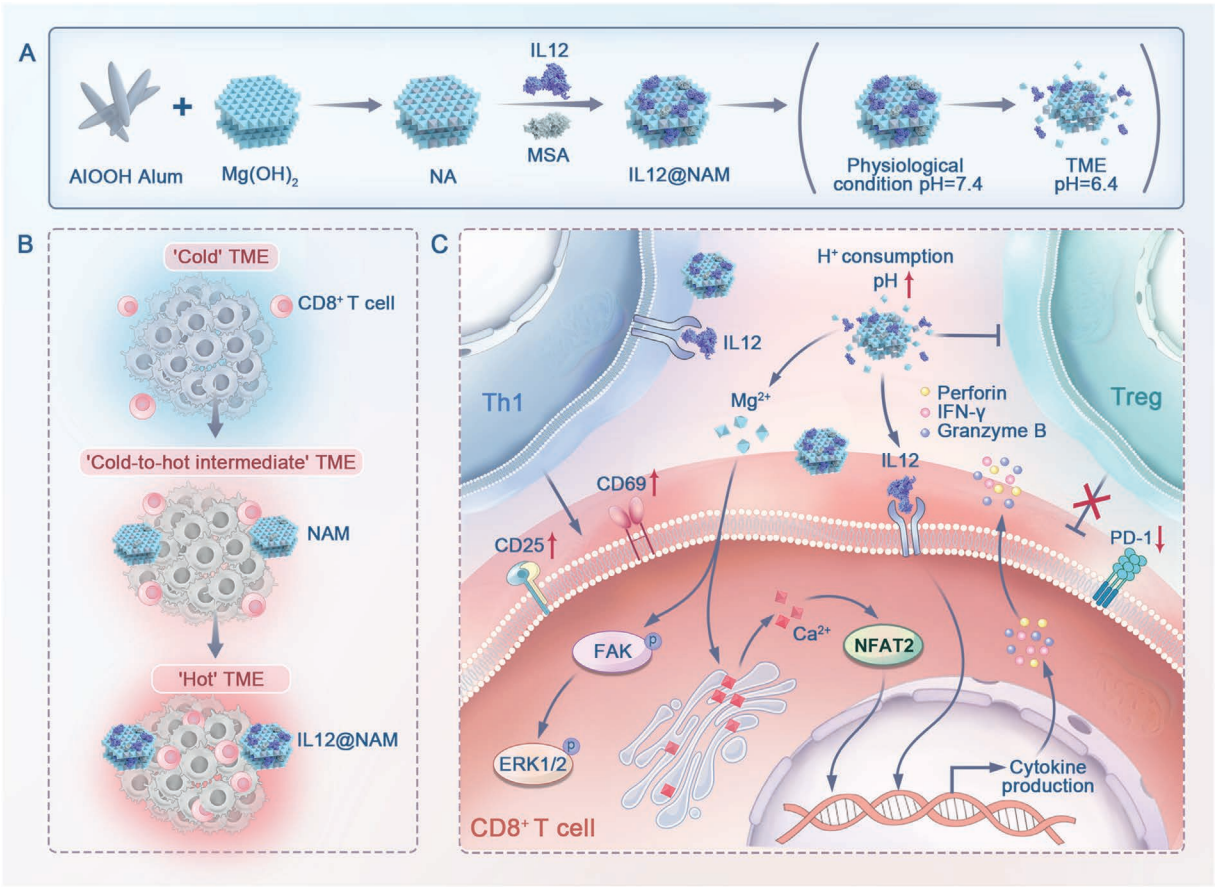

Scheme 1 Mechanistic illustration of IL12@NAM for promoting $CD8^+$ T cell activation while reducing exhuastion in the TME. (A) Schematic representation of IL12@NAM preparation and its acid-responsive release of Mg^{2+} and IL12. (B) Following peritumoral injection, IL12@NAM promotes $CD8^+$ T cell infiltration into deep tumor tissues. (C) Released Mg^{2+} enhances $CD8^+$ T cell activation *via* phosphorylation of FAK and ERK1/2 while synergizing with the Ca^{2+}−NFAT pathway, leading to augmented T cell activation including CD69 and CD25 and cytotoxic cytokines release. Additionally, H^+ neutralization and IL12/Mg^{2+} release alleviate immunosuppression by inhibiting Tregs and promoting Th1 $CD4^+$ T cell differentiation. This further reduces $CD8^+$ T cell exhaustion by downregulating PD1 expression.

2-mercaptoethanol, 2 mmol/L of L-glutamine, and 1 mmol/L of sodium pyruvate with anti CD3/CD28 antibodies.

2.3. *Animals*

All animal experiments in this work were performed according to protocols approved by Animal Care and Use Committee in the Shenzhen Bay Laboratory, China (SZBL) (officially approved animal ethics number: AEXZP202302). The female C57BL/6 mice (6−8 weeks old) and female BALB/c mice (6−8 weeks old) were purchased from Gempharmatech (China) and kept in a specific pathogen free (SPF), temperature-controlled and light-cycled animal facility. The *OT-I* mice (C57BL/6-Tg*(TcraTcrb) 1100Mjb/J*) were purchased from Geneandpeace (China).

2.4. *Animal treatment*

Female C57BL/6 mice (6−8 weeks old) were inoculated subcutaneously onto the right flanks with 2×10^5 of B16F10 melanoma cells (suspended in 100 μL saline) at Day 0. The tumors were measured every two days after Day 6.

The tumor volume was calculated according to Eq. (1):

$$\text{Volume} = 1/2 \times \text{Length} \times \text{Width}^2 \quad (1)$$

When the tumor reached a volume of 400 mm^3, the mice were peritumorally injected of 200 μL of saline dispersed with the following indicated formulations per mouse, including: G1: saline, G2: IL12 (2.5 μg), G3: NAM (1 mg), G4: IL12@NAM (2.5 μg of IL12 and 1 mg of NAM). Mice were sacrificed when then tumor volume reached 1500 mm^3, and tumors were collected for further analysis.

Female BALB/c mice (6−8 weeks old) were inoculated subcutaneously onto the right flanks with 1×10^6 of 4T1 cells (suspended in 100 μL saline) at Day 0. When the tumor volume reached 200 mm^3, the mice were peritumorally injected of 200 μL of saline dispersed with indicated formulations per mouse, including G1: saline, G2: IL12 (2.5 μg), G3: NAM (1 mg), G4: IL12@NAM (2.5 μg of IL12 and 1 mg of NAM). The tumors were collected at Day 24 for further analysis.

Female C57BL/6 mice (6−8 weeks old) were inoculated subcutaneously onto the right flanks with 2×10^5 of B16F10/OVA cells (suspended in 100 μL PBS) to construct B16F10/OVA tumor mice at day 0. OT-I $CD8^+$ T cells were isolated from the spleen and lymph nodes of *OT-I* mice and purified by $CD8^+$ T cells magnetic isolation kit. The $CD8^+$ T cells were stimulated with

peptide ($OVA_{257-264}$, 40 μg mL^{-1}) for 48 h. When the tumor volume reached 100 mm^3, mice received treatments in the following groups. T1: peritumoral injection with saline (200 μL); T2: mice retro-orbital injection (r.o.i.) with OT-I $CD8^+$ T cells (3×10^6 of cells in 100 μL of saline); T3: peritumoral injection with NAM (1 mg dispersed in 200 μL of saline) + r.o.i with OT-I $CD8^+$ T cells (3×10^6 of cells in 100 μL of saline); T4: peritumoral injection with IL12@NAM (2.5 μg of IL12 and 1 mg of NAM in 200 μL of saline) + r.o.i with OT-I $CD8^+$ T cells (3×10^6 of cells in 100 μL of saline) per mouse. The tumors were collected at Day 16 for further analysis.

2.5. Preparation and characterization of IL12@NAM

NA was synthesized through classical hydrothermal method. Briefly, 10 mL of mixed salt solution containing $MgCl_2 \cdot 6H_2O$ (0.3 mol/L) and $AlCl_3 \cdot 9H_2O$ (0.1 mol L^{-1}) was added to 40 mL of NaOH (0.2 mol L^{-1}) under vigorous stirring for 30 min. The slurry was then collected *via* centrifugation (4750×*g* for 15 min) and washed twice with 40 mL of deionized water. The slurry was dispersed with 40 mL of deionized water and hydrothermally treated at 100 °C for 16 h.

To increase colloidal stability, NA was added dropwise into mouse serum albumin (MSA) solution and stirred for 30 min to obtain NAM. The IL12@NA was prepared by adding IL12 dropwise into NA suspension and stirred for 15 min. The IL12@NA was subsequently added into MSA solution and stirred at room temperature for another 15 min to obtain IL12@NAM. The RITC-IL12@NA was obtained by dropwise adding RITC (Rhodamine B)-labelled IL12 into the NA suspensions and stirring for 15 min. Then the suspension was subsequently added into MSA solution and stirred for 15 min to obtain RITC-IL12@NAM. The MSA:NA mass ratio was fixed at 5:1 and the IL12:NA mass ratio at 1:400.

To determine the absorption of IL12 onto NA, 1 mL of NA (2 mg mL^{-1}) was dropwise added to 1 mL of IL12 solution (0.625, 1.25, 2.5, or 5 mg mL^{-1}) under an unltrasound bath for 5 min. Then the mixture was centrifuged at 15,000×*g* for 10 min and the concentration of IL12 in the supernatant was detected by a BCA kit (Yeasen, Shanghai, China). The Langmuir adsorption model ($Qe = QmCe/(1/K + Ce)$) was used to estimate the maximum IL12 adsorption capacity of NA (Ce: equilibration concentration of IL12 (mg mL^{-1}), Qe: equilibration amount of IL12 adsorbed by NA (mg g^{-1}), Qm: maximum monolayer adsorption amount (mg g^{-1}), K: adsorption equilibrium constant (mL mg^{-1}) estimated by fitting the adsorption isotherms). Based on these results, IL12@NAM was prepared using a similar procedure at 0.0025 mg (IL12)/mg (NA).

The morphology of NA and IL12@NAM was imaged in a transmission electron microscopy (TEM, JEOL JEM-F200, Japan). The element composition of NA and IL12@NAM was determined using inductively coupled plasma mass spectrometry (ICP-MS, Agilent 720 ES, USA). The X-ray diffraction pattern was recorded in Oxford Diffraction Gemini Ultra dual source CCD diffractometer (UK). The size and the zeta potential of NA, NAM and IL12@NAM was determined by dynamic light scattering (Malvern Instrument, USA).

2.6. pH detection

To detect the pH of NA solution, the NA was diluted with deionized water to the concentration ranging from 0 to 1000 μg mL^{-1}. To analyse the resistance of NA to acidification, the B16F10 cells (3×10^6 of cells per well) were seeded in a 12 well plate with 2 mL of culture medium in each well. The concentration of NAM was adjusted to 200 μg mL^{-1} in medium. The culture medium was collected every 12 h for 2 days and centrifuged at 800×*g* for 5 min to remove the cells. The pH was detected using a pH meter (OHAUS Starer 5000, USA).

2.7. Mg^{2+} and IL12 release from IL12@NAM

To assess the release of Mg^{2+} and IL12 from IL12@NAM in buffers with different pH (5.4, 6.4 and 7.4), IL12@NAM was diluted to 100 μg mL^{-1} in PBS at room temperature. The released Mg^{2+} and IL12 in the supernatant was collected at different time points. The collected supernatant was centrifuged at 15,000×*g* for 15 min to remove any IL12@NAM. The Mg^{2+} concentration was determined using ICP-MS (Agilent 720 ES, USA) and the IL12 concentration by Mouse IL12p70 enzyme-linked immunosorbent assay (ELISA) kit (SEKM-0013, Solarbio, China).

2.8. Analysis of distribution and clearance of peritumorally injected IL12@NAM in vivo

Cy5-IL12@NAM (200 μL, 2.5 μg of IL12 and 1 mg of NAM), Cy5-IL12 (200 μL, 2.5 μg of IL12) or saline was peritumorally injected into mice when the tumors reached ∼400 mm^3. The mice were imaged by *in vivo* Imaging System (IVIS Spectrum, USA) within 6 days to observe the fluorescence intensity in tumor areas. The *ex vivo* fluorescence images of the major organs and tumors were also recorded. The tumors were further sectioned for analysing the distribution of IL12 in the tumor tissue through fluorescence imaging in Olympus VS200 (EVIDENT, Japan).

NAM (200 μL, 1 mg per mouse) was peritumorally injected into melanoma mice when the tumors reached ∼400 mm^3. The tumor tissues were collected at Days 1 and 6 after treatment and dissolved with aqua regia for 24 h to fully lyse the tissues. The concentration of Mg^{2+} in the tumor lysis was analyzed using ICP-MS (Agilent 720 ES, USA).

2.9. Analysis of pH in tumor tissues post injection

To assess the acid-buffering capacity of IL12@NAM *in vivo*, B16F10 tumor-bearing mice (∼400 mm^3) were peritumorally injected with 200 μL of saline containing 1 mg of IL12@NAM. After 24 h, mice were intravenously injected with SNARF-1 (250 μg kg^{-1}, dissolved in 200 μL saline). At 30 min post injection, tumors were harvested, bisected, and subjected to fluorescence imaging using *in vivo* Imaging System. The pH values of all tumor tissues were determined from the radiometric emission of SNARF-1 at 580 and 640 nm.

2.10. Analysis of side effects in vivo

To assess the side effects of IL12@NAM in mice, the blood samples were collected at Day 4 after the peritumoral injection. The sera were collected from blood samples by resting at room temperature for 2 h and centrifuging at 2500×*g* for 20 min. The cytokines in the serum were quantified by the LegendPlex Mouse Inflammation Panel and analyzed by flow cytometry (Cytoflex, USA). The hematology analysis of blood samples was conducted in Auto Hematology Analyzer (Mindray, Shenzhen, BC-5000, China) including white blood cells and red blood cells. The

biochemistry analysis of serum samples was performed in Clinical Chemistry Analyzer (Mindray, BS-240, China) including aspartate aminotransferase (AST) and alanine aminotransferase (ALT).

2.11. Analysis of tumor infiltration of immune cells in vivo

The tumor tissues were collected post treatment with IL12, NAM and IL12@NAM. The tumors and spleens were cut into pieces of ~5 mm in size and digested in RPIM 1640 medium with 5% (*v*/*v*) of FBS, 0.5 mg mL^{-1} of Collagenase IV, and 100 IU/mL of DnaseI at 37 °C for 1 h for single cell dissociation. The red blood cells were removed using the red blood cell lysis buffer for 5 min. The tumor cell suspension was strained *via* a 70-μm cell sieve and stained with fluorescence-labelled anti-mouse antibodies to analyse the level of immune cells in tumor tissues. The cells were analyzed through flow cytometry (CytoFlex LX, Beckman and Auroroa, USA).

The spleen tissues were collected post treatment. The spleen cell suspension was stimulated with TRP2 (40 μg mL^{-1}) in an incubator at 37 °C with 5% (*v*/*v*) of carbon dioxide for 48 h. The cells were stained with fluorescence-labelled anti-mouse antibodies and analyzed through flow cytometry (CytoFlex LX, Beckman and Auroroa, USA).

2.12. Tissue immunofluorescence and immunocytochemistry analysis

The tumors in melanoma mice were collected at 4 days post treatment. Tissues were fixed in 10% paraformaldehyde and embedded in paraffin for sectioning. The CD8 fluorescence staining was conducted to analyse the immune infiltration in tumors. The TUNEL staining was performed to assess the tumor apoptosis. The hematoxylin an eosin (H&E) staining was performed to assess the tissue morphology in major organs. The IFN-γ staining was conducted to analyse the cytokine expression in tumors. The histological analysis was performed using Imgae J software.

2.13. Calcium flux analysis

The $CD8^+$ T cells were isolated from mouse spleens and lymph modes and purified using the magnetic isolation kit. The $CD8^+$ T cells were stained with Fluo-4 dyes at the concentration of 4 μmol/L for 30 min at 37 °C. The cells were washed twice and diluted into 1×10^6 cell mL^{-1} in PBS. The cells were collected to analyse the Fluo-4 signal for 30 s as the baseline. The $CD8^+$ T cells were then stimulated with anti CD3/CD28 and IL12@NAM for 3 s, and their Fluo-4 signal was recorded for another 270 s.

2.14. Activation, exhaustion and gene expression analysis of $CD8^+$ T cells

The $CD8^+$ T cells were isolated from mouse spleens and lymph modes and monitored by flow cytometry. The $CD8^+$ T cells were seeded in the CD3/28 antibodies pre-coated 96 well plate. The IL12@NAM (100 μg mL^{-1}) was added and cultured for 8 h. The CD25, CD69, *p*-ERK1/2 and *p*-FAK expression of cells were measured.

For exhaustion analysis, the $CD8^+$ T cells were stimulated in the CD3/CD28 antibodies pre-coated 96 well plate for 2 days. Then IL12@NAM (100 μg mL^{-1}) was added and cultured for another 3 days. The PD1 and LAG3 expression of cells were measured every day for 5 days.

For gene expression analysis, the $CD8^+$ T cells were stimulated in the CD3/CD28 antibodies pre-coated 96 well plate for 48 h and then cocultured with IL12@NAM (100 μg mL^{-1}) for 3 days. The gene expression of these T cells was analyzed using qPCR (QuantStudio 5.0, Thermo Fisher, USA). The primer sequences are listed in Supporting Information Table S3.

2.15. Statistical analysis

Data are presented as the mean ± standard error of the mean (SEM) based on at least triplicate experiments. The means were analyzed by one-way or two-way analysis of variance as indicated, followed by multiple comparisons using Tukey's test within the Prism software package (Prism 10.2.1; GraphPad Software, USA, 2024).

3. Results and discussion

3.1. Characteristics of IL12@NA

The TEM image shows that NA hydrothermally reengineered from the mixture of AlOOH and $Mg(OH)_2$ at an initial molar ratio of 3:1 exhibited typical hexagonal morphology, with elements Mg, Al, and O evenly distributed in the layers (Fig. 1A)[13]. The X-ray diffraction pattern confirms its layered crystal structure (evidenced by the characteristic *003*, *006*, *009*, *110* and *113* peaks; Fig. 1B), and the Mg/Al molar ratio of NA was 2.94 as determined by ICP-MS. These results indicate that the successful crystal recombination of AlOOH and $Mg(OH)_2$ and formation of layered NA. To prepare IL12@NAM, IL12 was loaded onto the NA surface first through electrostatic adsorption and the outstanding protein adsorption capacity ensures the complete loading of IL12 (Supporting Information Fig. S1). Then MSA was then adsorbed to coat positively charged NA to maintain colloidal stability. Surface coating with IL12 and albumin did not change the morphology, crystal structure and element distribution of NA (Fig. 1C and D). However, the surface charge decreased from 42.0 ± 0.9 mV of NA to 40.0 ± 1.8 mV of IL12@NA (IL12:NA mass ratio of 0.25:100) after IL12 loading (Fig. 1D), indicating that a small portion of the positively charged surface of NA was occupied by IL12[27]. Meanwhile, the particle size increased from 66.6 ± 0.1 nm of NA to 116.1 ± 0.7 nm of IL12@NA (Fig. 1D). When the positively charged surface of IL12@NA was coated with negatively charged MSA (IL12@NAM), the particle size of IL12@NAM slightly decreased to 103.3 ± 1.8 nm and the zeta potential further decreased to −16.4 ± 0.3 mV (Fig. 1D). The adsorption of MSA significantly increased the stability of IL12@NAM by preventing the potential bridge-linking effect between particles. As a result, the resultant IL12@NAM exhibited excellent dispersity in culture medium containing 10% of FBS for 24 h, compared to IL12@NA (Fig. 1E).

NA inherits the weak alkalinity from the Mg-based layered structure (*e.g.*, $Mg(OH)_2$), where partial hydrolysis of Mg^{2+}-containing hydroxide layers results in OH^- release (*e.g.*, $Mg(OH)_2 \rightarrow Mg^{2+} + 2OH^-$). Thus, the pH of IL12@NA solution increased in a concentration-dependent manner and reached 9−10 at 50−200 μg mL^{-1} (Supporting Information Fig. S2). Subsequently, the incubation of IL12@NAM (200 μg mL^{-1}) with B16F10 cells elevated the culture medium pH by 0.3−0.4 unit

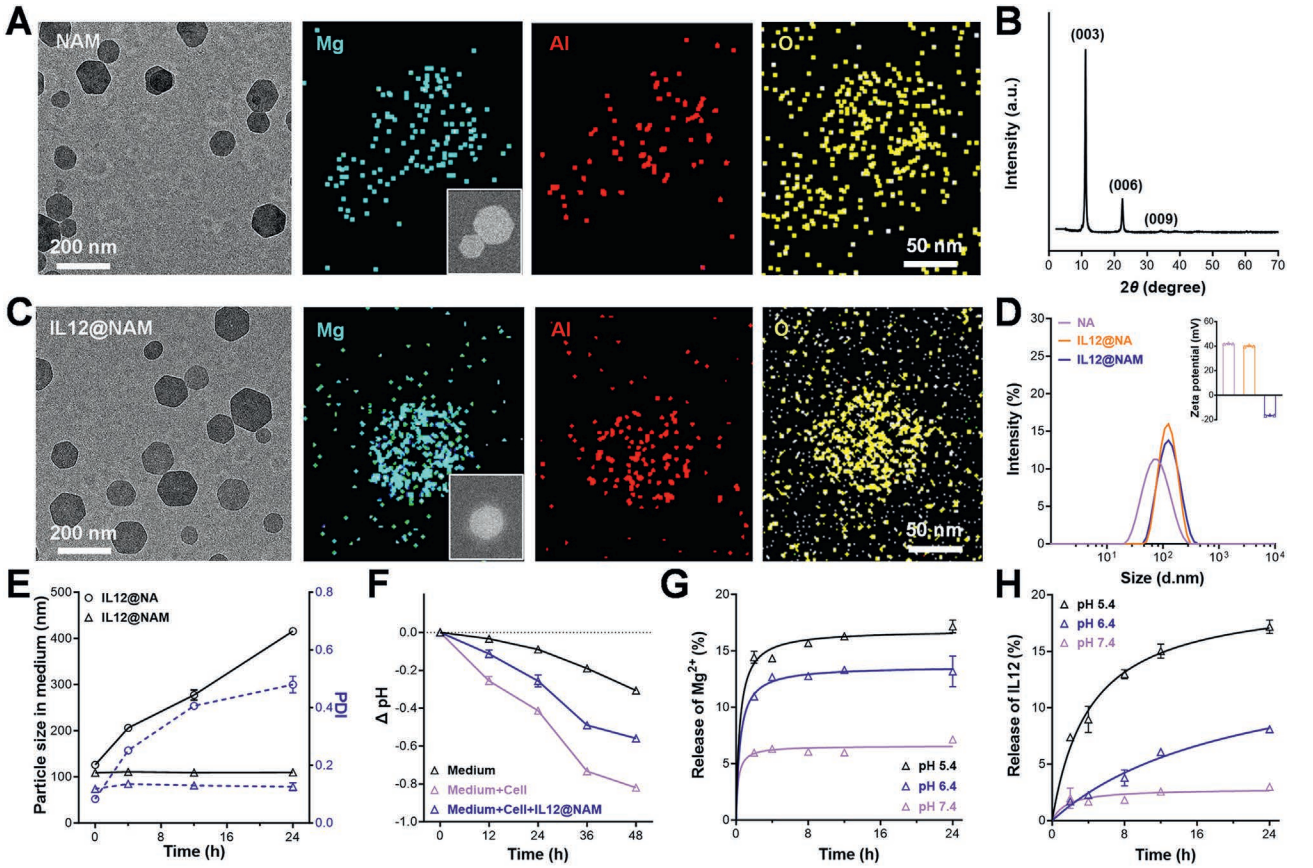

Figure 1 Characteristics of prepared IL12@NAM. (A) TEM image and element mapping of NAM in energy dispersive X-ray spectroscopy. (B) XRD pattern of NA. (C) TEM image and element mapping of IL12@NAM. (D) Particle size distribution and zeta potential of NA-based samples. (E) Colloidal stability of IL12@NAM and IL12@NA in culture medium supplemented with 10% of FBS was monitored by the average particle size and PDI over 24 h. (F) pH variations of culture media in 24-well plates seeded with B16F10 cells in the presence or absence of IL12@NAM. (G) Mg^{2+} release profile of IL12@NAM determined using ICP-MS. (H) IL12 releases profile of IL12@NAM determined using ELISA, $n = 3$ wells in (D−H). Data are presented as the mean ± SEM.

after 36−48 h incubation (Fig. 1F), suggesting IL12@NAM effectively neutralized the lactic acid produced by tumor cells. To test the release of Mg^{2+} and IL12 during the acid neutralization, IL12@NAM was dispersed in buffers that mimic the pH of TME (6.4) and lysosome (5.4), respectively. The release of Mg^{2+} in pH 7.4 buffer within 2 h was only 6.5%, mainly resulting from the spontaneous hydrolysis of NA (Fig. 1G). This process was significantly enhanced in acidic buffers, as 13.2% and 17.2% of total Mg^{2+} was burst released within the first 2 h in pH 6.4 and 5.4 buffers and then maintained almost unchanged due to the reach of dissolution-precipitation balance (Fig. 1G). Similarly, release of IL12 was largely associated with the dissolution of NA. Under physiological conditions (pH 7.4), an ignorable amount of IL12 (<2%) was released from IL12@NAM after 24 h. In sharp contrast, IL12 was sustainably released from IL12@NAM in the acidic buffers, as around 8% and 17% was detected in pH 6.4 and 5.4 buffers for 24 h, respectively (Fig. 1H and Supporting Information Fig. S3). Moreover, the treatment of IL12@NAM significantly elevated $CD8^+$ T cell-mediated cytotoxicity against tumor cells by enhanced $CD8^+$ T cells activation, compared with IL12+NAM prepared by simply mixing NAM with free IL12 (Supporting Information Fig. S4). This is because less IL12 could be adsorbed onto the negatively charged surface of MSA-coated NAM after simple mixing. Collectively, IL12@NAM showcases promising potential in neutralizing acidic TME while responsively supplementing Mg^{2+} and IL12 to improve the killing efficiency of $CD8^+$ T cells.

3.2. *Biocompatible IL12@NAM neutralizes acid in the TME and supplements Mg^{2+} and IL12*

To evaluate the accumulation and retention as well as Mg^{2+} and IL12 supplement in the TME, IL12@NAM was administered peritumorally to advanced (∼400 mm^3) B16F10 tumor-bearing mice. The *in vivo* fluorescence monitoring revealed that the fluorescence of Cy5-IL12@NAM gradually decreased but remained strong around tumor tissues over 6 days. In contrast, free Cy5-IL12 rapidly disappeared from tumor tissue and was very weak at Day 3 (Fig. 2A and B, Supporting Information Fig. S5A). The *ex vivo* fluorescence imaging further showed that IL12@NAM remained at tumor tissues even after 6 days of peritumoral injection, but with minimal accumulation observed in the liver (Fig. 2C and D, Fig. S5B and S5C). Importantly, the acidic tumor pH was elevated to the physiological level at 24 h following peritumoral injection of IL12@NAM (Fig. 2E and F). During this period, Mg^{2+} and IL12 were released from IL12@NAM due to the dissolution of NA. Approximately 38% of the injected Mg^{2+} (in both ionic and particulate forms) was detected in tumor tissues

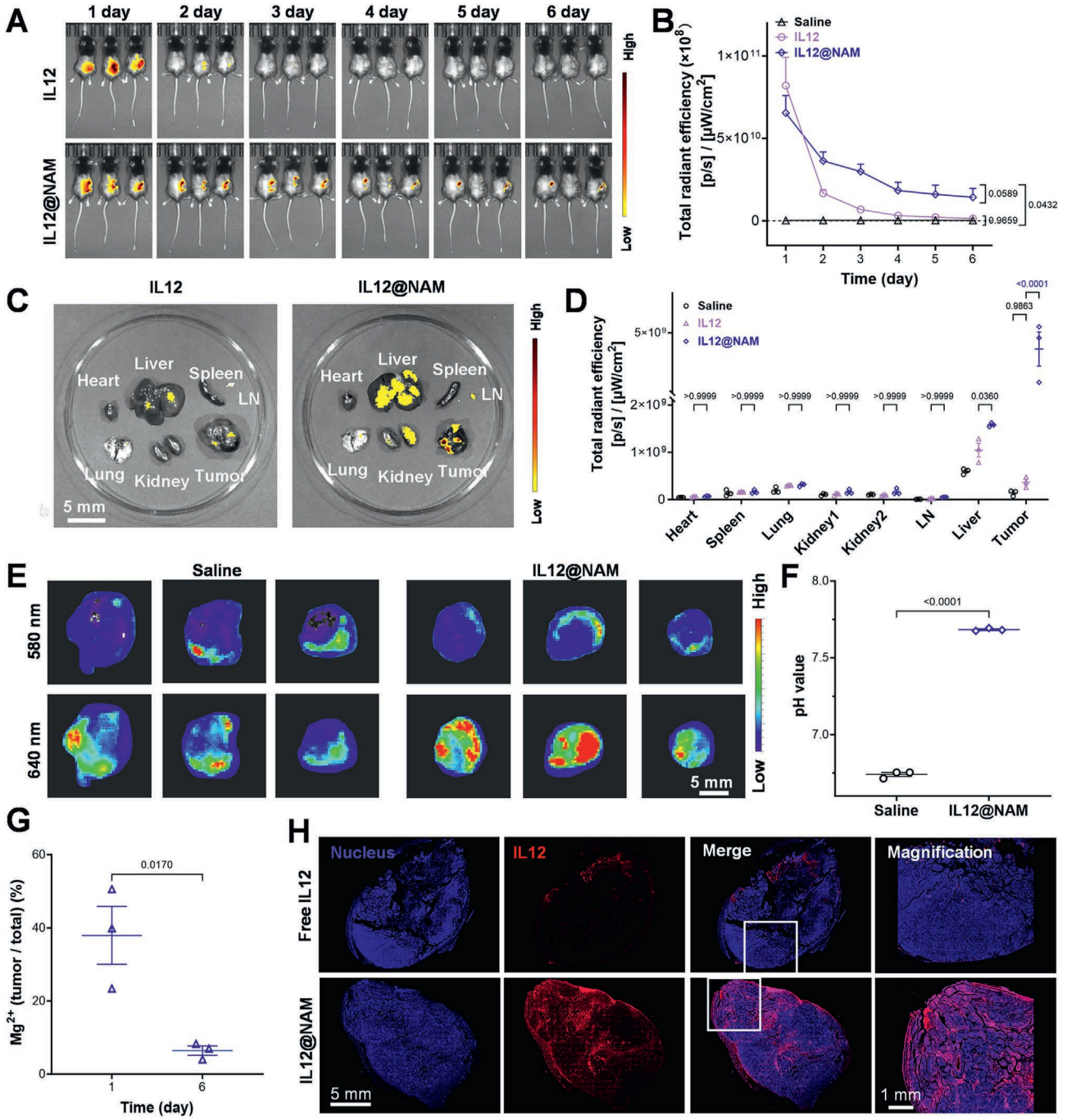

Figure 2 IL12@NAM neutralizes acid and supplies Mg^{2+} and IL12 in TME. (A) B16F10 tumor-bearing mice peritumorally injected with free IL12 or IL12@NAM (IL12 labelled with Cy5). The retention of IL12@NAM around the tumor tissues was monitored using the *in vivo* Imaging System for 6 days. (B) Digitalized data of the fluorescence intensity in (A). (C) *Ex vivo* fluorescence images of the major organs and tumors of mice treated with free IL12 or IL12@NAM (IL12 labelled with Cy5) collected at Day 6 post-injection. (D) Digitalized data of the fluorescence intensity in (C). (E) SNARF-1 fluorescence images (read at 580 and 640 nm) of tumors treated with IL12@NAM for 24 h. (F) The estimated pH values of tumors in (E) calculated from the fluorescence intensity ratio (I_{580}/I_{640}). (G) The resident Mg^{2+} percent (tumor-associated Mg^{2+} to total Mg^{2+} in injected IL12@NAM) was detected by ICP-MS. (H) IL12 and IL12@NAM distribution in the tumor tissues (IL12 labelled with RITC) after peritumoral injection to tumor-bearing mice. After 24 h, the tumors were collected and sectioned for analyzing the distribution of IL12 by Olympus ($n = 3$ mice per group). Scale bar = 5 mm (main image) and 1 mm (magnified area). Data are presented as the mean ± SEM. The *P* values were analyzed by one-way analysis of variance, followed by multiple comparisons using Tukey's test.

at 24 h post-injection, which was decreased to 6% after 6 days (Fig. 2G), in consistent with the *in vivo* and *ex vivo* fluorescence images (Fig. 2A−D). This indicates that IL12@NAM continuously stayed and infiltrated in tumor tissues and was gradually consumed over time. Furthermore, free IL12 was found to rapidly dissipate from tumor tissues, whereas IL12 delivered by IL12@NAM effectively infiltrated into solid tumors, distributing evenly across both the tumor margin and central region (Fig. 2H).

On this basis, the biosafety of IL12@NAM was assessed in B16F10 melanoma-bearing mice. Given the inflammatory toxicity associated with IL12 in clinical applications, serum cytokine levels were analyzed[28]. Peritumoral injection of IL12 alone significantly elevated serum inflammatory cytokines, including IFN-γ (a direct downstream molecule of IL12)[23,29], IL6, IL1α, and IL1β. In contrast, the controlled release of IL12 around the tumors *via* IL12@NAM dramatically reduced the serum IFN-γ level (Supporting Information Fig. S6). Moreover, peritumoral injection of free IL12 led to an increase in serum levels of AST and ALT, both of which are hallmarks of hepatotoxicity. By comparison, the serum levels of AST and ALT in IL12@NAM-treated mice were comparable to those in saline-treated mice (Supporting Information Fig. S7). Notably, treatment with IL12@NAM significantly prevented IL12-induced lymphopenia[30]. Complete blood count analysis showed that levels of white blood cells, lymphocytes, neutrophils, eosinophils, and monocytes remained within the normal range in IL12@NAM treated group (Supporting Information Fig. S8A−S8E). Additionally, IL12@NAM treatment restored the level of red blood cells and neutrophils to the normal range, counteracting the decrease caused by cancer cells (Fig. S8F)[31,32]. Further analysis using H&E staining of the major organs (kidney, lung, spleen, liver and heart) revealed no significant pathological abnormalities in IL12@NAM treated mice (Supporting Information Fig. S9). Correspondingly, no body weight loss was observed in the IL12@NAM-treated group (Supporting Information Fig. S10). Collectively, these results demonstrate that IL12@NAM is a highly biosafe agent for the local delivery of IL12 for solid tumor therapy.

3.3. *IL12@NAM recruits and activates CD8$^+$ T cells*

To determine the optimal mass ratio of IL12: NA, CD8$^+$ T cell mediated cytotoxicity assay against the tumor was performed *in vitro* using a range of IL12: NA mass ratios (1: 200, 1: 400, and 1: 800). The data revealed that IL12@NAM at 1: 400 induced the highest tumor-killing activity (Supporting Information Fig. S11). Moreover, IL12@NAM at 1: 400 exhibited the lowest PD1 expression, leading to reduced exhaustion. Therefore, 1: 400 is the most effective ratio for enhancing T cell cytotoxic activity.

Peritumorally supplemented Mg^{2+} and IL12 by IL12@NAM have been observed to significantly enhance the recruitment and activation of CD8$^+$ T cells within the TME. A single peritumoral injection of free IL12 to advanced ($\sim$400 mm^3) B16F10 tumor-bearing mice did not obviously increase the level of CD8$^+$ T cells in tumor tissues (G2) compared to the saline treatment group (G1) (Fig. 3A and Supporting Information Fig. S12). In stark contrast, a single injection of IL12@NAM (G4) significantly increased the level of CD8$^+$ T cells in tumors, reaching approximately 2.0−2.6 times that observed in saline- or free IL12-treated groups (Fig. 3A). The level of chemokine CXCL9 (facilitates CD8$^+$ T cell recruitment)[33-35] was observed the highest in IL12@NAM treated tumors, which was around 3 times that in IL12 or NAM treated tumors (Supporting Information Fig. S13). Therefore, IL12@NAM demonstrated superior efficacy in recruiting CD8$^+$ T cells from around and the tumor edge into deeper tissues compared to IL12 or NAM treatment alone (Fig. 3B). At the same time, IL12@NAM treatment led to a significant increase in the levels of perforin and granzyme B in CD8$^+$ T cells (CD8$^+$ Perforin$^+$ and CD8$^+$ Granzyme$^+$ T cells) (Fig. 3C and D, Supporting Information Fig. S14). Notably, among the CD8$^+$ T cells recruited in tumor tissues, the level of memory effector CD8$^+$ T cells (CD8$^+$ CD44$^+$ CD62L$^-$ T cells) was the highest in IL12@NAM treatment group, being around 2.1−2.3 times that treated with free IL12 or NAM (Fig. 3E and Supporting Information Fig. S15).

The enhanced CD8$^+$ T cell recruitment and activation are largely attributed to the synergistic immunomodulation between Mg^{2+} and IL12. In NAM- or IL12@NAM-treated CD8$^+$ T cells, the released Mg^{2+} was observed to participate in downstream FAK (proximal signal) and ERK1/2 (distal signal) phosphorylation, following the interaction between Mg^{2+} and LFA1 (Fig. 3F and G, Supporting Information Fig. S16)[36]. In sharp contrast, IL12 treatment alone did not change the phosphorylation of FAK and ERK1/2, while free Mg^{2+} (concentration similar to that in NAM, G5) only increased the phosphorylation of FAK (Fig. 3F and G, Fig. S16). As a result, effective activation of CD8$^+$ T cells was observed in groups treated with NAM and IL12@NAM, especially the levels of CD69 (an early activation marker) and CD25 (a late activation marker) being 2.3−3.0 times that in cells treated with saline (Fig. 3H and I, Supporting Information Fig. S17). This activation is primarily attributed to the supplied Mg^{2+} rather than IL12, as the expression of CD69 and CD25 in CD8$^+$ T cells treated with IL12 was nearly identical to that in cells treated with saline.

Benefiting from the same charge in the replacement of Ca^{2+} in endoplasmic reticulum (ER) by Mg^{2+}[37], addition of Mg^{2+} in free form or by hydrolysis from NAM rather than IL12 was observed to increase the ER Ca^{2+} release in CD8$^+$ T cells (Fig. 3J), thereby contributing to activation of the Ca^{2+}−NFAT pathway[38,39]. Increased cytoplasm Ca^{2+} in both IL12 and NAM-treated CD8$^+$ T cells slightly elevated the expression of *Nfatc1* (encodes NFAT2 and controls the cytotoxicity and memory differentiation of CD8$^+$ T cells)[40,41], compared with that in saline-treated group (Fig. 3K). Excitedly, the synergy between Mg^{2+}-mediated ER Ca^{2+} release and IL12 significantly increased the expression NFATc1 in CD8$^+$ T cells to 3.6 times that in saline-treated group (Fig. 3K). As a result, dramatical increase of *Ifn-γ* expression (3.7 times that in saline-treated group) was observed in CD8$^+$ T cells treated with IL12@NAM due to potent activation of the Ca^{2+}−NFAT pathway (Fig. 3L). Collectively, the synergy between Mg^{2+} and IL12 effectively recruits CD8$^+$ T cells to filtrate into solid tumors and promotes their activation, cytotoxicity and memory differentiation (Fig. 3M).

3.4. *IL12@NAM reduces CD8$^+$ T cell exhaustion*

Continuous exposure to anti-CD3/CD28 stimulation was observed to elevate the expression of PD1, an early exhaustion marker in CD8$^+$ T cells (Supporting Information Fig. S18A and S18B). As shown in Fig. 4A, both IL12 and NAM treatments effectively reduced PD1 expression in CD8$^+$ T cells[42]. IL12 treatment significantly increased the expression of LAG3, a marker associated with late T cell exhaustion (Fig. 4B and Fig. S18C)[43]. In sharp contrast, NAM treatment markedly decreased LAG3 expression in CD8$^+$ T cells (Fig. 4B). Consequently, an overall

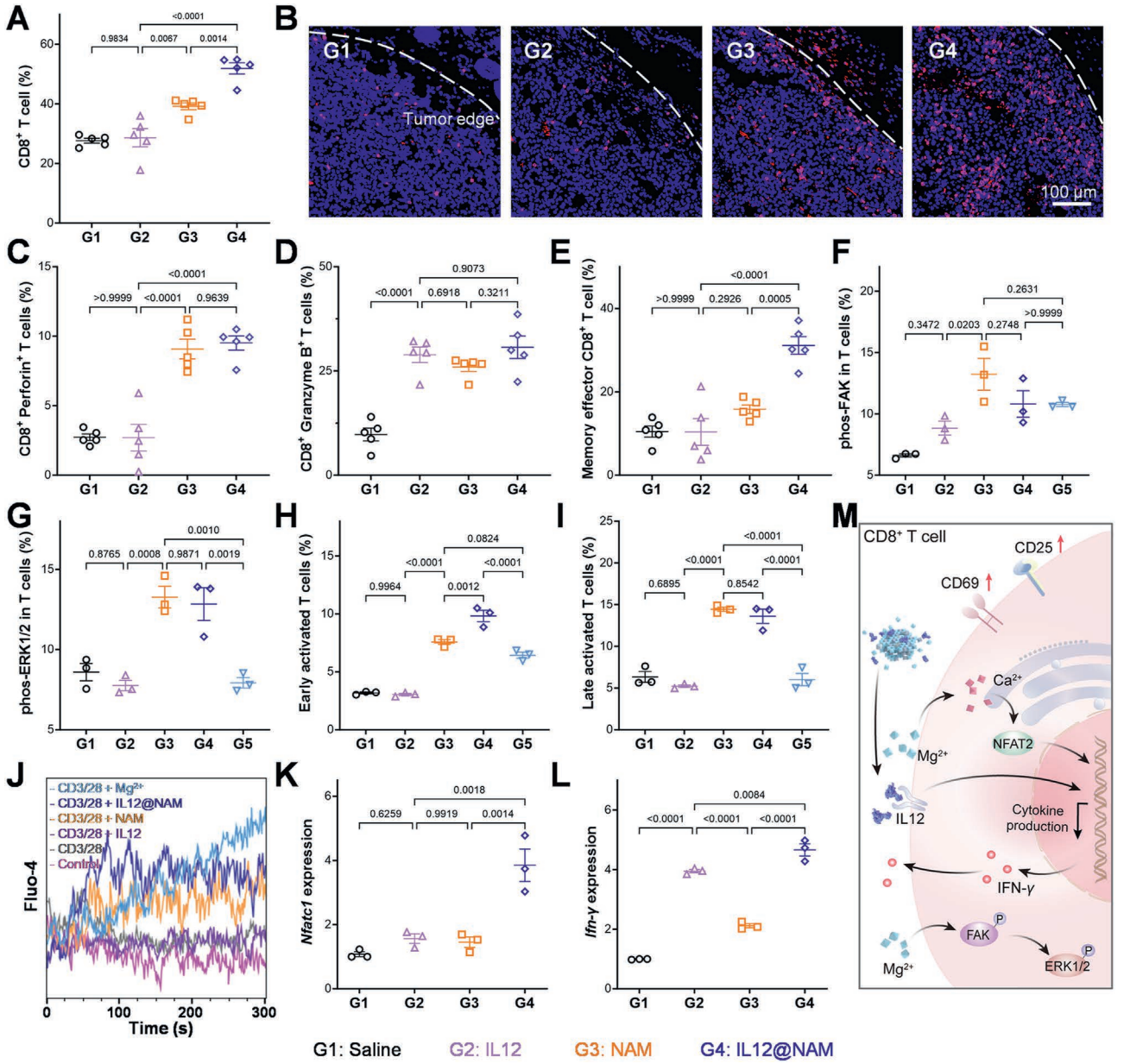

Figure 3 IL12@NAM enhances CD8$^+$ T cell recruitment and activation. CD8$^+$ T cells or tumors were treated as follows: G1, Saline; G2, IL12; G3, NAM; G4, IL12@NAM. (F–I) G5: Mg^{2+} treatment (1 mmol/L, similar to the content in NAM). (A, B) CD8$^+$ T cell (gating on CD8$^+$ in CD3$^+$) infiltration in B16 tumor tissues measured by flow cytometry (A) and immunofluorescence (B). Scale bar = 100 μm. (C, D) The level of Perforin$^+$ (C) and Granzyme B$^+$ (D) CD8$^+$ T cells in tumor tissues. (E) The level of memory effector T cells (gating on CD44$^+$ CD62L$^-$ in CD8$^+$ T cells) in tumor tissues (n = 5 mice per group in (A–E)). (F, G) The expression of phos-FAK (F) and phos-ERK1/2 (G) in CD8$^+$ T cells with *ex vivo* treatment measured by flow cytometry. (H, I) The level of early (H) and late (I) activated T cells with *ex vivo* treatment. (J) Ca^{2+} flux triggered by anti CD3/CD28 stimulation in CD8$^+$ T cells. (K, L) *Nfatc1* and *Ifn-γ* expression with indicated *ex vivo* treatments measured by qPCR (n = 3 wells per group in (F–L)). (M) Schematic diagram of T cell activation by IL12@NAM. Data are presented as the mean ± SEM. The P values were analyzed by one-way analysis of variance, followed by multiple comparisons using Tukey's test.

analysis of CD8$^+$ T cell exhaustion revealed that IL12@NAM effectively reduced the proportion of late-exhausted CD8$^+$ T cells (PD1$^{+/-}$ LAG3$^+$) in comparison with IL12 treatment, *i.e.* from 61.9% in the IL12-treated group to 41.2% in the IL12@NAM-treated group (Fig. 4C and Supporting Information Fig. S19).

Interestingly, the normalization of tumor pH, combined with continuous IL12 supplementation, significantly reshaped the CD4$^+$ T cell populations within the TME, further contributing to the alleviation of CD8$^+$ T cell exhaustion. Both IL12 and IL12@NAM treatments notably increased the total proportion of CD4$^+$ T cells in tumors (Fig. 4D and Supporting Information Fig. S20). Specifically, the proportions of activated CD4$^+$ T cells (CD4$^+$ CD69$^+$ CD25$^-$) in IL12-and IL12@NAM-treated cells were 1.9 to 2.5 times that in saline-treated group (Fig. 4E and Supporting Information Fig. S21). Moreover, IL12@NAM

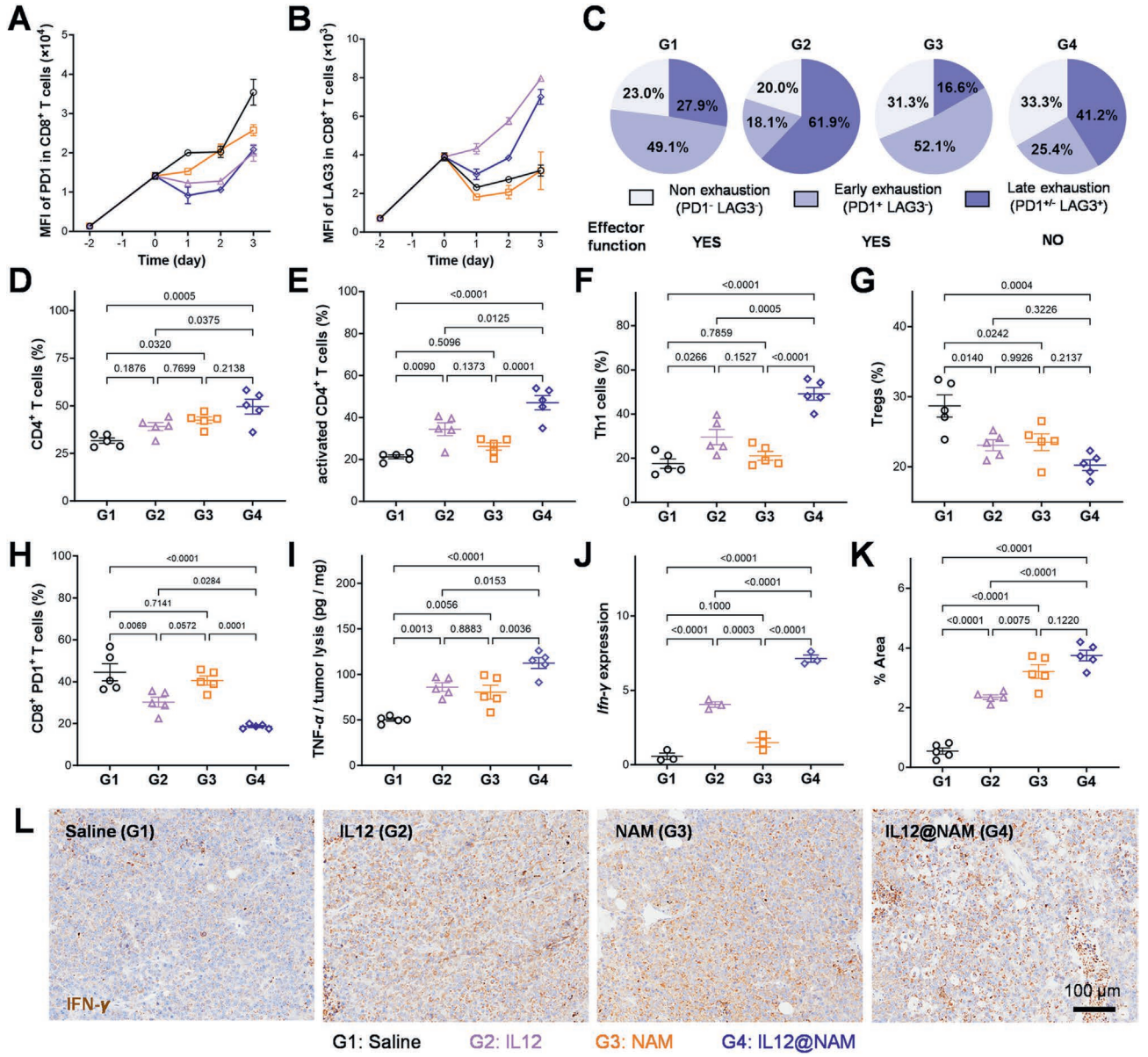

Figure 4 IL12@NAM remodels the T cell immunity in TME. $CD8^+$ T cells or tumors were treated as follows: G1, saline; G2, IL12; G3, NAM; G4, IL12@NAM. (A, B) The expression level of PD1 (A) and LAG3 (B) in $CD8^+$ T cells after *ex vivo* treatment along with anti CD3/CD28 over time measured by flow cytometry. (C) The non- ($PD1^-LAG3^-$), early- ($PD1^+LAG3^-$) and late- ($PD1^{+/-}LAG3^+$) exhausted $CD8^+$ T cells measured by flow cytometry 24 h after indicated treatments ($n = 3$ wells per group). (D−G) Levels of $CD4^+$ T cells (gating on $CD4^+$ in $CD3^+$(D), activated $CD4^+$ T cells (gating on $CD69^+CD25^-$ in $CD4^+$) (E), Th1 cells (gating on T-BET^+ in $CD4^+$) (F) and Tregs (gating on $FoxP3^+$ in $CD4^+$) (G) in tumors from tumor-bearing mice, measured by flow cytometry. (H) The PD1 expression in $CD8^+$ T cells of tumor tissues analyzed by flow cytometry. (I) The level of TNF-α in tumors at the indicated times measured by ELISA ($n = 5$ mice per group in (D−I)). (J) *Ifn-γ* expression by $CD8^+$ T cells after 72 h *ex vivo* treatment measured by qPCR ($n = 3$ wells per group). (K, L) The level of IFN-γ in tumors measured by immunohistochemistry (L) and quantification (K) ($n = 5$ mice per group). Scale bar = 100 μm. Data are presented as the mean ± SEM. The *P* values were analyzed by one-way analysis of variance, followed by multiple comparisons using Tukey's test.

most effectively promoted the differentiation of T helper 1 (Th1) cells ($CD4^+$ T-BET^+) (Fig. 4F and Fig. S21). Concurrently, the level of Tregs ($CD4^+$ $FoxP3^+$) was the lowest in IL12@NAM-treated tumors, likely due to the neutralization of the acidic TME by NAM and IL12 effects (Fig. 4G and Supporting Information Fig. S22)[13,15]. As a result, the level of $CD8^+$ $PD1^+$ T cells was the lowest in IL12@NAM-treated tumors (Fig. 4H and Supporting Information Fig. S23). Meanwhile, IL12@NAM treatment significantly elevated the levels of pro-inflammatory cytokines in the TME (Fig. 4I−L). Collectively, the pro-inflammatory effects of IL12, combined with the tumor pH neutralization capacity of NAM, effectively increased the proportion of Th1 cells, which is essential for promoting $CD8^+$ T cell survival, memory response, tumor localization and cytotoxicity[44]. Simultaneously, this combination also reduced the level of Tregs, thus reducing $CD8^+$ T cell exhaustion[45]. In addition, IL12@NAM also functioned as an

in-situ vaccine adjuvant, capturing tumor antigens released from dying tumor cells. The increased natural killer (NK) cell infiltration within the tumor suggests an effective early antitumor response mediated by innate immunity (Supporting Information Fig. S24A). Together with the tumor killing by $CD8^+$ T cells, the released tumor antigens from the dead tumor cells induced robust dendritic cell activation in tumor-draining lymph nodes and the generation of Trp2-specific $CD8^+$ T cells in the splenocytes of mice treated peritumorally with IL12@NAM (Fig. S24B and S24C). Thus, beyond directly activating $CD8^+$ T cells, IL12@NAM effectively remodels the $CD4^+$ T cell populations within the TME, creating a favorable immunological milieu to empower the functions of $CD8^+$ T effector cells.

3.5. IL12@NAM directly inhibits the progression of advanced solid tumors

To further evaluate whether IL12@NAM effectively enhances the suppression of solid tumors by activating $CD8^+$ T cells and mitigating their exhaustion, advanced ($\sim$400 mm^3) B16F10 melanoma-bearing mice were established and treated with IL12@NAM *via* peritumoral injection (Fig. 5A). Notably, mice treated with saline had to be euthanized at Day 16 as their tumor volumes exceeded 1500 mm^3. At this time point, the tumor suppression efficiency in mice treated with IL12@NAM was approximately 68%, which was significantly higher than 33% observed with IL12 treatment and 50% with NAM treatment (Fig. 5B and C). The superior tumor suppression efficiency observed with NAM, compared to IL12, is largely attributed to the prolonged retention of NAM for neutralization of the excess acid within tumor tissues, whereas free IL12 is rapidly cleared from the tumor site and/or degraded. By contrast, the combination of IL12 and NAM in IL12@NAM enabled sustained tumor growth inhibition, as the excess acid was neutralized (Fig. 2F) and the IL12 was sustainably released (Fig. 2H) within tumor tissues. Consistently, the terminal deoxynucleotidyl transferase dUTP nick end labelling (TUNEL) assay demonstrated that IL12@NAM treatment significantly enhanced apoptosis in tumor tissues, especially in the core region (Fig. 5D). This finding suggests that IL12@NAM effectively recruits and activates $CD8^+$ T cells to target and eliminate tumor cells in the deeper region of the tumor tissues.

Moreover, the therapeutic efficacy of IL12@NAM in mitigating tumor metastasis was further evaluated using a 4T1 breast cancer mouse model, with peritumoral injection of the indicated formulations to advanced ($\sim$250 mm^3) solid tumors (Fig. 5E). Similarly, IL12@NAM exhibited potent tumor suppression, achieving a 54% inhibition at Day 24. In stark contrast, tumor suppression achieved by IL12 and NAM treatment was only 19% and 34%, respectively (Fig. 5F and G). Consistently, the superior control of tumor progression by IL12@NAM significantly delayed tumor metastasis, as evidenced by fewer tumor nodules in the lungs (Fig. 5H). In summary, peritumoral injection of IL12@NAM is very potent in effectively inhibiting primary solid tumor growth and preventing potential tumor metastasis, but its application in hematological malignancies without the tumor microenvironment may not be possible.

3.6. IL12@NAM amplifies the therapeutic efficacy of adoptive T cells

To assess the *in vivo* fate of adoptively transferred T cells, DiR-labelled $CD8^+$ T cells were administered into B16F10 tumor-bearing mice ($\sim$100 mm^3). At Day 3 post injection, the *ex vivo* fluorescence images proved a significantly elevated fluorescence signal of tumor tissues, indicating successful infiltration and retention of transferred T cells in the TME (Supporting Information Fig. S25). To assess whether IL12@NAM-mediated $CD8^+$ T cell recruitment and activation in the TME improve adoptive cell therapy, OT-I $CD8^+$ T cells, which specifically recognize OVA, were transfused *via* retro-orbital injection into B16F10-OVA-bearing mice that were pre-treated 1 day early with peritumorally injection of the indicated formulations (Fig. 6A). This process was repeated once 4 days later. Treatment with OT-I $CD8^+$ T cells alone slightly inhibited tumor growth, achieving a tumor suppression efficiency of only 18% at Day 16 (Fig. 6B and C). In contrast, the combination of OT-I T cell transfusion and peritumoral NAM treatment resulted in a higher tumor suppression (56%) (Fig. 6B and C), again demonstrating the contribution of excess acid neutralization in the TME to T cell therapy. Excitedly, together with OT-I $CD8^+$ T cells, IL12@NAM, which combined the advantages of IL12 and NAM, significantly inhibited the progression of B16F10-OVA tumors, achieving a tumor suppression up to 90% at Day 16 (Fig. 6B and C). Importantly, no significant body weight loss was observed in the combination therapy group (Supporting Information Fig. S26).

The immunological analysis revealed that peritumoral administration of IL12@NAM significantly increased the infiltration of both $CD8^+$ and $CD4^+$ T cells within the TME (Fig. 6D). Specifically, peritumoral treatment with IL12@NAM dramatically elevated the level of $CD8^+$ T cells in tumors to 21.1% from 2.4% with OT-I transfusion alone and 7.2% with NAM treatment (Fig. 6E and Supporting Information Fig. S27), suggesting that IL12 and NAM synergistically recruited $CD8^+$ T cells into solid tumors. Moreover, IL12@NAM most efficiently enhanced $CD8^+$ T cell proliferation ($Ki67^+$ $CD8^+$ T cells) (Fig. 6F and Supporting Information Fig. S28). In consistence with previous findings, IL12@NAM not only increased the cytotoxicity of $CD8^+$ T cells, reflected by elevated levels of $Perforin^+$, $Granzyme\ B^+$, and $IFN\text{-}\gamma^+$ $CD8^+$ T cells (Fig. 6G–I and Supporting Information Fig. S29), but also reduced their exhaustion, as evidenced by decreased expression of PD1 (Fig. 6J–L and Supporting Information Fig. S30). The increased proliferation of $CD4^+$ T cells ($Ki67^+$ in $CD4^+$) within the tumor likely supported $CD8^+$ T cell responses (Supporting Information Fig. S31). Furthermore, the elevated population of effector $CD8^+$ T cells ($CD44^+CD62^-$ in $CD8^+$) and the higher proportion of MHCII DCs ($IA\text{-}IE^+H2Kb^-$ in $CD45^+CD11c^+$) in tumor-draining lymph nodes (tdLNs) indicate enhanced antigen presentation and more efficient effector differentiation (Supporting Information Fig. S32). Collectively, these findings demonstrate that IL12@NAM creates a favorable microenvironment for the recruitment, activation, enhanced cytotoxicity and decreased exhaustion of OT-I $CD8^+$ T cells, thereby effectively controlling the progression of solid tumors.

In summary, IL12@NAM has elegantly combined the environmental and immunological modulation to synergically empower T cells in the TME. The former modulation involves the neutralization of excess acid and relieves the notorious acidosis, preparing an immunoresponsive environment to well maintain the functions of infiltrated T cells (*e.g.*, activation, proliferation, and cytotoxicity). The latter modulation stimulates infiltration and activation of $CD8^+$ and $CD4^+$ T cells in the TME by sustainably providing Mg^{2+} and IL12[46]. Complementarily, the environmental modulation mitigates $CD8^+$ T cell exhaustion that is often induced by directly supplied IL12, but both modulations together effectively increase the Th1 cell population and decrease regulatory T

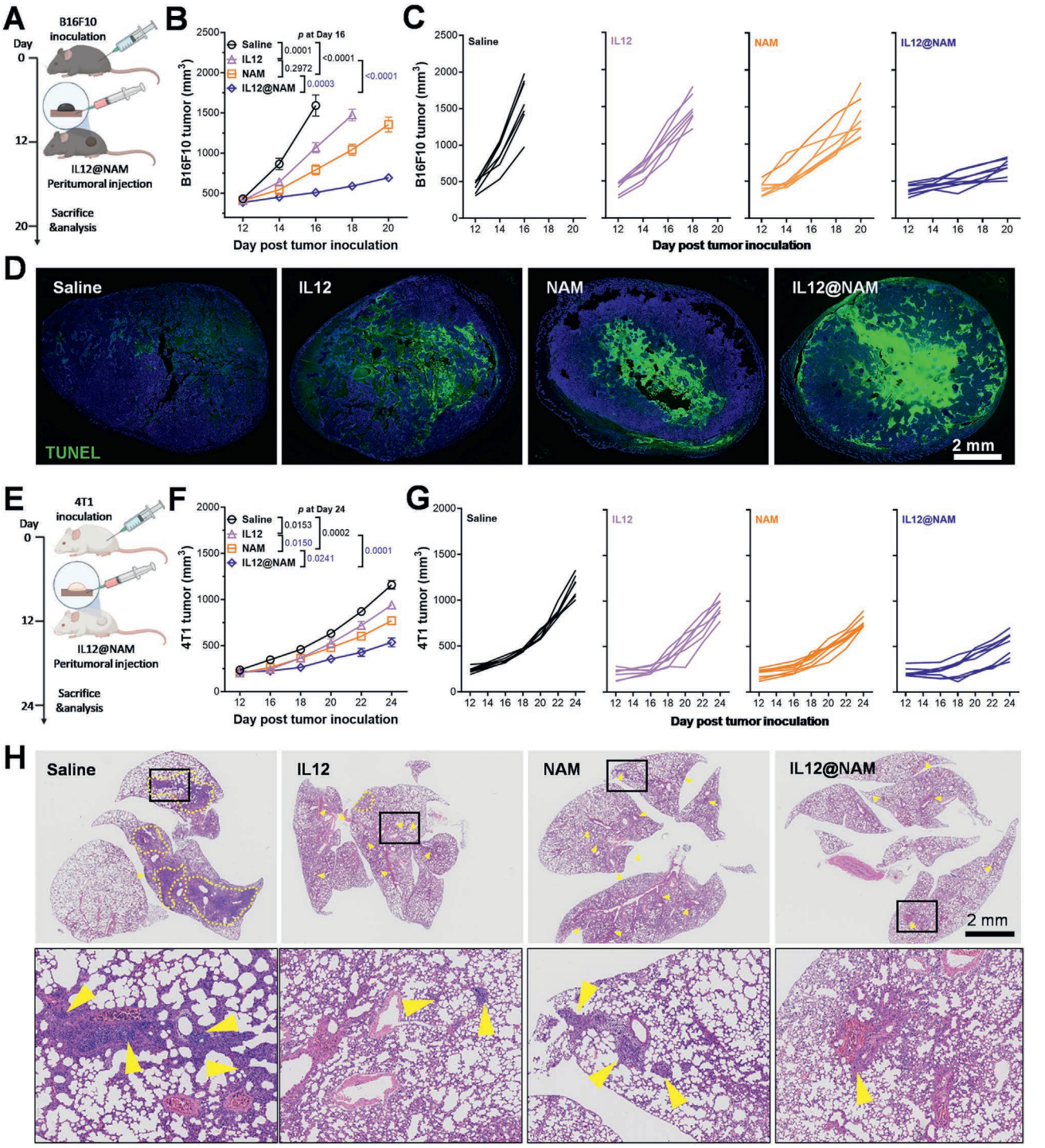

Figure 5 IL12@NAM treatment directly inhibits melanoma and breast cancer progression. Tumor-bearing mice were treated as follows: saline; IL12; NAM; IL12@NAM. (A) Schematic illustration of the therapeutic procedure of B16F10 melanoma mice. (B, C) The average (B) and individual (C) volume of melanoma was measured every two days (n = 7 or 8 mice per group). (D) TUNEL staining of melanoma tumors. Scale bar = 2 mm. (E) Schematic illustration of the therapeutic procedure of 4T1 breast cancer mice. (F, G) The average (F) and individual (G) volume of breast cancer were measured every two days (n = 7 mice per group). (H) H&E staining of lungs collected at Day 24 for analyzing tumor metastasis. Scale bar = 2 mm. Data are presented as the mean ± SEM. The P values were analyzed by two-way analysis of variance, followed by multiple comparisons using Tukey's test.

cells. Therefore, IL12@NAM treatment restores a more favorable immune microenvironment and network for enhanced $CD8^+$ T cell-mediated anti-tumor immunity. Such an investigation is different from other studies that focus on either augmenting the abundance and activity of anti-tumor immune cells to alleviate immunosuppressive TME[47,48], or normalizing the TME

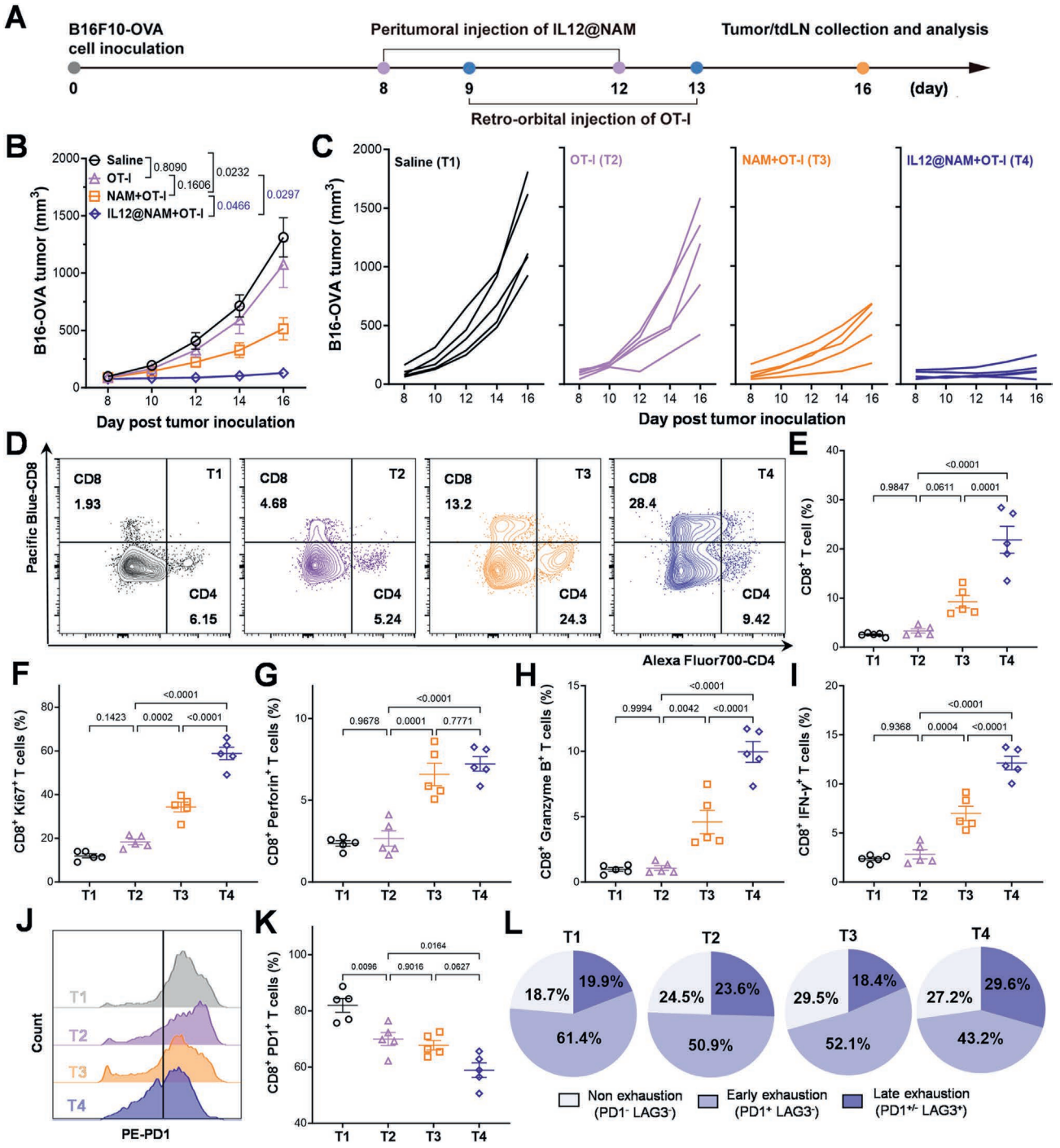

Figure 6 Therapeutic effects of OT-1 $CD8^+$ T cells in combination with IL12@NAM on B16F10-OVA melanoma. Tumor-bearing mice were treated as follows: T1, saline; T2, OT-I; T3, NAM + OT-I; T4, IL12@NAM + OT-I. (A) Schematic of the therapeutic procedure for B16F10-OVA melanoma mice. (B, C) The average (B) and individual (C) volumes of the melanoma tumor were measured every two days. (D, E) Representative flow cytometry plots (D) and corresponding quantification (E) of $CD8^+$ T cells. (F–I) The level of $Ki67^+$ (F), $Perforin^+$ (G), Granzyme B^+ (H), and IFN-γ^+ (I) in $CD8^+$ T cells of tumors measured by flow cytometry. (J, K) Representative histograms (J) and quantified expression (K) of PD1 in tumors measured by flow cytometry. (L) The level of non- ($PD1^-LAG3^-$), early- ($PD1^+LAG3^-$) and late- ($PD1^{+/-}LAG3^+$) exhausted $CD8^+$ T cells in tumors). Data are presented as the mean ± SEM (n = 5 mice per group). The P values were analyzed by two-way analysis of variance, followed by multiple comparisons using Tukey's test.

physicochemical properties (low pH and hypoxia)[13,49,50]. This is why dual-functional IL12@NAM effectively bolsters the responses of T cells, thus holding significant potential to transform the therapeutic landscape for solid tumors.

4. Conclusions

TME significantly impedes the efficacy of T cell-based therapies due to factors like acidosis and nutrient metal ion imbalance. In

this study, we developed IL12@NAM to enhance T cell effector function within the immunosuppressive TME. Peritumorally injected IL12@NAM were mostly retained at the injection site, which gradually diffused into tumor tissues, neutralizing excess acid and releasing IL12 and Mg^{2+}. Different from conventional IL12 delivery systems, NAM used in this study not only delivered and maintained IL12 within the tumor tissues for a long time but also normalized the immunosuppressive factors, such as acidosis and Mg^{2+} deficiency, that inactivate $CD8^+$ T cell function. First, the supplemented Mg^{2+} promoted $CD8^+$ T cell activation *via* the LFA1−NFAT2 pathway. Then, the gradually released IL12 from IL12@NAM further amplified the NFAT2-mediated activation process in $CD8^+$ T cells. The synergy between Mg^{2+} and IL12 activates and ensures sufficient cytotoxic $CD8^+$ T cells in tumor tissues. Moreover, neutralization of excess acid in tumor tissues by NAM significantly decreased the Treg level and promoted Th1 polarization of $CD4^+$ T cells, which greatly alleviated the inactivation of the activated $CD8^+$ T cells. Meanwhile, intracellularly released IL12 also decreased the expression of PD1 and LAG3 in $CD8^+$ T cells and reduced their exhaustion. Thus, the anti-acid and Mg^{2+} supplementation of NAM enables it to create a favorable microenvironment to maintain the effector function of $CD8^+$ T cells. As a result, IL12@NAM significantly improved cytotoxicity of $CD8^+$ T cells that are inherently reside in the tumor tissues or enter from the peripheral blood, being an ideal candidate for cancer adjuvant therapy. This will be further benefited from the combination of IL12@NAM and clinical tumor ablation techniques, which enable direct, high-dose, multi-site injection of IL12@NAM into deep-seated tumors at once or a few times to achieve local delivery and amplify therapeutic efficacy. Despite this, the application of IL12@NAM for hematological malignancies may be achieved by using it for *in vitro* adoptive T cell expansion or *in vivo* T cell immune modulation through appropriate particle modification. Nevertheless, the designed IL12@NAM in this study presents a novel paradigm for effective and safe cytokine-based tumor T cell therapy.

Acknowledgements

This work was financially supported by grants from the European Union's Research and Innovation Program under the Marie Skłodowska-Curie grant agreement (Grant 101064861, Europe), the Natural Science Foundation of Ningbo Municipality (Grant 2022J273, China), Shenzhen Bay Laboratory Startup Grant (Z.P. Xu) and Hangzhou City University Starting Grant (L. Zhang).

Author contributions

Aining Shen and Jing Zhao equally performed the experiments, contributed to the methodology, development, analyzed the data, prepared the figures, and wrote the initial draft of the manuscript. Zhenwei Su, contributed to the methods and analysis of the preparation of IL12@NAM and the regulation of T cells. Ran Wang, contributed the immunological analysis of T cells. Ying Li, Chaojie Zhu, Qingyuan Zhao and Pinwan Yu contributed to the animal experiments. Zhi Ping Xu, contributed to the conceptualization of the study, designed the experiments, supervised the execution of the *in vivo* experimental work, contributed to the interpretation of the data, and reviewed the manuscript. Lingxiao Zhang, contributed to the conceptualization of the study, designed the experiments, supervised the execution of the experimental work and data analysis, contributed to the interpretation of the data, and prepared, reviewed, and revised the manuscript.

Conflicts of interest

The authors declare no conflicts of interest.

Appendix A. Supporting information

Supporting information to this article can be found online at https://doi.org/10.1016/j.apsb.2025.10.021.

References

1. Deckers J, Anbergen T, Hokke AM, de Dreu A, Schrijver DP, de Bruin K, et al. Engineering cytokine therapeutics. *Nat Rev Bioeng* 2023;**1**:286−303.
2. Dall'Olio FG, Marabelle A, Caramella C, Garcia C, Aldea M, Chaput N, et al. Tumour burden and efficacy of immune-checkpoint inhibitors. *Nat Rev Clin Oncol* 2022;**19**:75−90.
3. Low V, Li Z, Blenis J. Metabolite activation of tumorigenic signaling pathways in the tumor microenvironment. *Sci Signal* 2022;**15**: eabj4220.
4. DePeaux K, Delgoffe GM. Metabolic barriers to cancer immunotherapy. *Nat Rev Immunol* 2021;**21**:785−97.
5. Shi W, Liu N, Lu H. Advancements and challenges in immunocytokines: a new arsenal against cancer. *Acta Pharm Sin B* 2024;**14**: 4649−64.
6. Watson MJ, Vignali PDA, Mullett SJ, Overacre-Delgoffe AE, Peralta RM, Grebinoski S, et al. Metabolic support of tumour-infiltrating regulatory T cells by lactic acid. *Nature* 2021;**591**:645−51.
7. Li Y, He C, Shen AN, Wang Y, Xu ZP, Zhang L, et al. pH of Microenvironment directly modulates the phenotype and function of cancer-associated fibroblasts. *ACS Omega* 2025;**10**:3937−43.
8. Zhang J, Li J, Hou Y, Lin Y, Zhao H, Shi Y, et al. Osr2 functions as a biomechanical checkpoint to aggravate $CD8^+$ T cell exhaustion in tumor. *Cell* 2024;**187**:P3409-26.E24.
9. Lötscher J, Martí ILAA, Kirchhammer N, Cribioli E, Giordano Attianese GMP, Trefny MP, et al. Magnesium sensing *via* LFA-1 regulates $CD8^+$ T cell effector function. *Cell* 2022;**185**:585−602.e29.
10. Ma J, Tang L, Tan Y, Xiao J, Wei K, Zhang X, et al. Lithium carbonate revitalizes tumor-reactive $CD8^+$ T cells by shunting lactic acid into mitochondria. *Nat Immunol* 2024;**25**:552−61.
11. Moskowitz A, Lee J, Donnino MW, Mark R, Celi LA, Danziger J. The association between admission magnesium concentrations and lactic acidosis in critical illness. *J Intensive Care Med* 2016;**31**:187−92.
12. Zhu C, Jiang J, Jia Y, Xu ZP, Zhang L. Beyond drug delivery system: immunomodulatory layered double hydroxide nanoadjuvants take an essential step forward in cancer immunotherapy. *Acc Mater Res* 2023; **4**:758−71.
13. Zhang L, Jia Y, Yang J, Zhang L, Hou S, Niu X, et al. Efficient immunotherapy of drug-free layered double hydroxide nanoparticles *via* neutralizing excess acid and blocking tumor cell autophagy. *ACS Nano* 2022;**16**:12036−48.
14. Jia Y, Hu J, Zhu C, Li Z, Yang X, Liu R, et al. Engineered NanoAlum from aluminum turns cold tumor hot for potentiating cancer metalloimmunotherapy. *J Control Release* 2023;**354**:770−83.
15. Zhang L, Bai J, Shen A, Zhao J, Su Z, Wang M, et al. Artificially tagging tumors with nano-aluminum adjuvant-tethered antigen mRNA recruits and activates antigen-specific cytotoxic T cells for enhanced cancer immunotherapy. *Biomaterials* 2025;**317**:123085.

16. Tugues S, Burkhard SH, Ohs I, Vrohlings M, Nussbaum K, Vom Berg J, et al. New insights into IL-12-mediated tumor suppression. *Cell Death Differ* 2015;**22**:237−46.
17. Vom Berg J, Vrohlings M, Haller S, Haimovici A, Kulig P, Sledzinska A, et al. Intratumoral IL-12 combined with CTLA-4 blockade elicits T cell-mediated glioma rejection. *J Exp Med* 2013; **210**:2803−11.
18. Mukhopadhyay A, Wright J, Shirley S, Canton DA, Burkart C, Connolly RJ, et al. Characterization of abscopal effects of intratumoral electroporation-mediated IL-12 gene therapy. *Gene Ther* 2019;**26**: 1−15.
19. Mirlekar B, Pylayeva-Gupta Y. IL-12 family cytokines in cancer and immunotherapy. *Cancers (Basel)* 2021;**13**:167.
20. Li M, Lu L, Xiao Q, Maalim AA, Nie B, Liu Y, et al. Bioengineer mesenchymal stem cell for treatment of glioma by IL-12 mediated microenvironment reprogramming and nCD47-SLAMF7 mediated phagocytosis regulation of macrophages. *Exploration* 2024;**4**:20240027.
21. Luo Y, Chen Z, Sun M, Li B, Pan F, Ma A, et al. IL-12 nanochaperone-engineered CAR T cell for robust tumor-immunotherapy. *Biomaterials* 2022;**281**:121341.
22. Morris EC, Neelapu SS, Giavridis T, Sadelain M. Cytokine release syndrome and associated neurotoxicity in cancer immunotherapy. *Nat Rev Immunol* 2022;**22**:85−96.
23. Agarwal Y, Milling LE, Chang JYH, Santollani L, Sheen A, Lutz EA, et al. Intratumourally injected alum-tethered cytokines elicit potent and safer local and systemic anticancer immunity. *Nat Biomed Eng* 2022;**6**:129−43.
24. Li Y, Su Z, Zhao W, Zhang X, Momin N, Zhang C, et al. Multifunctional oncolytic nanoparticles deliver self-replicating *IL-12* RNA to eliminate established tumors and prime systemic immunity. *Nat Cancer* 2020;**1**:882−93.
25. Liu MR, Hu SQ, Yan N, Popowski KD, Cheng K. Inhalable extracellular vesicle delivery of *IL-12* mRNA to treat lung cancer and promote systemic immunity. *Nat Nanotechnol* 2024;**19**:565−75.
26. Du S, Yan J, Xue Y, Zhong Y, Dong Y. Adoptive cell therapy for cancer treatment. *Exploration* 2023;**3**:20210058.
27. Zhang LX, Zhao J, Hu X, Wang CH, Jia YB, Zhu CJ, et al. A peritumorally injected immunomodulating adjuvant elicits robust and safe metalloimmunotherapy against solid tumors. *Adv Mater* 2022;**34**: e2206915.
28. Mansurov A, Hosseinchi P, Chang K, Lauterbach AL, Gray LT, Alpar AT, et al. Masking the immunotoxicity of interleukin-12 by fusing it with a domain of its receptor *via* a tumour−protease−cleavable linker. *Nat Biomed Eng* 2022;**6**:819−29.
29. Dong S, Guo X, Han F, He Z, Wang Y. Emerging role of natural products in cancer immunotherapy. *Acta Pharm Sin B* 2022;**12**: 1163−85.
30. Portielje JE, Kruit WH, Schuler M, Beck J, Lamers CH, Stoter G, et al. Phase I study of subcutaneously administered recombinant human interleukin 12 in patients with advanced renal cell cancer. *Clin Cancer Res* 1999;**5**:3983−9.
31. Gilreath JA, Rodgers GM. How I treat cancer-associated anemia. *Blood* 2020;**136**:801−13.
32. Yuan T, Jia QZ, Zhu B, Chen DG, Long HX. Synergistic immunotherapy targeting cancer-associated anemia: prospects of a combination strategy. *Cell Commun Signal* 2023;**21**:117.
33. Bergamaschi C, Pandit H, Nagy BA, Stellas D, Jensen SM, Bear J, et al. Heterodimeric IL-15 delays tumor growth and promotes intratumoral CTL and dendritic cell accumulation by a cytokine network involving XCL1, IFN-γ, CXCL9 and CXCL10. *J Immunother Cancer* 2020;**8**:e000599.
34. Hu J, Sun C, Bernatchez C, Xia X, Hwu P, Dotti G, et al. T-cell homing therapy for reducing regulatory T cells and preserving effector T-cell function in large solid tumors. *Clin Cancer Res* 2018;**24**: 2920−34.
35. Ma C, Wong CK, Wong BCK, Chan KCA, Lun SWM, Lee N, et al. Cytokine responses in a severe case of glandular fever treated successfully with foscarnet combined with prednisolone and intravenous immunoglobulin. *J Med Virol* 2009;**81**:99−105.
36. Lotscher J, Marti ILAA, Kirchhammer N, Cribioli E, Giordano Attianese GMP, Trefny MP, et al. Magnesium sensing *via* LFA-1 regulates $CD8^+$ T cell effector function. *Cell* 2022;**185**:585−602.e29.
37. Baumann O, Walz B, Somlyo AV, Somlyo AP. Electron probe microanalysis of calcium release and magnesium uptake by endoplasmic reticulum in bee photoreceptors. *Proc Natl Acad Sci U S A* 1991;**88**:741−4.
38. Muller MR, Rao A. NFAT, immunity and cancer: a transcription factor comes of age. *Nat Rev Immunol* 2010;**10**:645−56.
39. Macian F. NFAT proteins: key regulators of T-cell development and function. *Nat Rev Immunol* 2005;**5**:472−84.
40. Klein-Hessling S, Muhammad K, Klein M, Pusch T, Rudolf R, Floter J, et al. NFATc1 controls the cytotoxicity of $CD8^+$ T cells. *Nat Commun* 2017;**8**:511.
41. Heim L, Friedrich J, Engelhardt M, Trufa DI, Geppert CI, Rieker RJ, et al. NFATc1 promotes antitumoral effector functions and memory $CD8^+$ T-cell differentiation during non-small cell lung cancer development. *Cancer Res* 2018;**78**:3619−33.
42. Kang S, Mansurov A, Kurtanich T, Chun HR, Slezak AJ, Volpatti LR, et al. Engineered IL-7 synergizes with IL-12 immunotherapy to prevent T cell exhaustion and promote memory without exacerbating toxicity. *Sci Adv* 2023;**9**:eadh9879.
43. Yang ZZ, Grote DM, Ziesmer SC, Niki T, Hirashima M, Novak AJ, et al. IL-12 upregulates TIM-3 expression and induces T cell exhaustion in patients with follicular B cell Non-Hodgkin lymphoma. *J Clin Investig* 2012;**122**:1271−82.
44. Huang H, Hao S, Li F, Ye Z, Yang J, Xiang J. $CD4^+$ Th1 cells promote $CD8^+$ Tc1 cell survival, memory response, tumor localization and therapy by targeted delivery of interleukin 2 *via* acquired pMHC I complexes. *Immunology* 2007;**120**:148−59.
45. Penaloza-MacMaster P. CD8 T-cell regulation by T regulatory cells and the programmed cell death protein 1 pathway. *Immunology* 2017; **151**:146−53.
46. Shao JH, Wang MZ, Huang JL, Wang Y, Zhao J, Wang R, et al. Biomimetic nanomedicines deliver Naringin for enhanced acute liver failure therapy *via* balanced regulation of hepatocyte oxidative stress and Kupffer cell inflammation. *Adv Funct Mater* 2025;**35**: 2502801.
47. Lopez de Rodas M, Villalba-Esparza M, Sanmamed MF, Chen L, Rimm DL, Schalper KA. Biological and clinical significance of tumour-infiltrating lymphocytes in the era of immunotherapy: a multidimensional approach. *Nat Rev Clin Oncol* 2025;**22**:163−81.
48. Zhang HB, Chen LL, Li L, Liu Y, Das B, Zhai S, et al. Prediction and analysis of tumor infiltrating lymphocytes across 28 cancers by TILScout using deep learning. *npj Precis Oncol* 2025;**9**:76.
49. Sun LY, Gao WD, Liu J, Wang JJ, Li L, Yu HJ, et al. O_2-supplying nanozymes alleviate hypoxia and deplete lactate to eliminate tumors and activate antitumor immunity. *ACS Appl Mater Interfaces* 2022;**14**: 56644−57.
50. Ding BB, Zheng P, Tan J, Chen H, Meng Q, Li J, et al. Sodium bicarbonate nanoparticles for amplified cancer immunotherapy by inducing pyroptosis and regulating lactic acid metabolism. *Angew Chem Int Ed Engl* 2023;**62**:e202307706.